Università degli Studi di Padova

Dipartimento di Fisica e Astronomia "Galileo Galilei"

Corso di Laurea in

Astronomia

The Delay Time of Merging Compact Objects

Relatore

Michela Mapelli

Università di Padova

Correlatore

Nicola Giacobbo

Candidato

Alberto Brentegani

Anno Accademico 2018/2019

Abstract

The advent of gravitational wave astronomy, with the observation of GW150914, urges us to study the formation and the evolution of compact object binary systems. Indeed, all gravitational waves emission events detected so far by LIGO and Virgo are linked to the coalescence of compact binary systems. This work focuses on the analysis of two simulations ran through the binary population-synthesis code MOBSE. The purpose of this analysis is to study the delay time, i.e. the interval of time before the coalescence event, measured starting from zero age main sequence. The delay time is a fundamental quantity to estimate the merger rate of compact binaries. In the first part of this work, we give an overview of the physical processes that occur during massive star evolution in a binary system framework and their impact on the formation of compact binary systems. In the second part, we perform the analysis of two binary population-synthesis simulations. The simulations are analyzed to evaluate the impact of metallicity and natal kicks on the delay time of compact object binaries.

Abstract

L'avvento dell'astronomia ad onde gravitazionali, con l'osservazione di GW150914, ci motiva ancora di più a studiare la formazione e l'evoluzione di sistemi binari di oggetti compatti. Infatti, tutti gli eventi di emissione di onde gravitazionali osservati finora da LIGO e Virgo sono associati alla coalescenza di sistemi binari di oggetti compatti. In particolare, il mio lavoro si concentra sull'analisi di due simulazioni effettuate tramite il codice di sintesi di popolazione MOBSE. Lo scopo di questa analisi è studiare il tempo di ritardo (delay time), ossia il tempo impiegato dalla binaria ad arrivare all'evento di coalescenza, misurato partendo dall'entrata delle stelle nella sequenza principale. Il delay time è una grandezza fondamentale per stimare il tasso di coalescenza (merger rate), ovvero il tasso di fusione dei sistemi di oggetti compatti. Nella prima parte di questa tesi, vengono descritti i processi fisici che avvengono durante la vita delle stelle massicce in sistemi binari e il loro impatto sulla formazione dei sistemi binari compatti. Nella seconda parte di questa tesi, viene condotta un'analisi originale su due campioni di simulazioni di sintesi di popolazione. Le simulazioni sono analizzate per valutare l'impatto della metallicità stellare e dei "natal kick" sul delay time dei sistemi binari compatti.

Contents

1 Introduction

On September 14, 2015, the LIGO interferometers captured a gravitational wave (GW) signal from a *black hole binary* (BHB) merger (see Abbott et al. [1]). This event, named GW150914, was the first detection of GWs and the first observation of a BHB merger. Following this detection the Virgo interferometer joined the second observation run, enabling the first three-detector observations of GWs. This milestone set the beginning of the GW astronomy, and added a fundamental element to the developing *multi-messenger astronomy*.

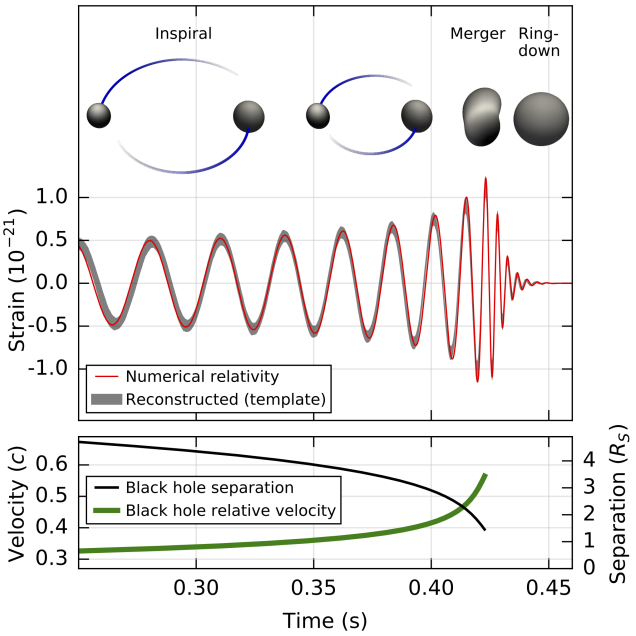

Figure 1: Results from the analysis of GW150914, taken from Abbott et al. [1]. *Top*: comparison of the observed GW strain with the prediction of the waveform computed from general relativity; images of the BH horizons at various stages of the merger are shown at the top. *Bottom*: plot velocity and separation of the two BHs as the merger event unfolds.

During the first and the second observation runs, nine more BHB mergers have been observed as shown in Table 1 (for a review of the two observation runs see Abbott et al. [2]). Furthermore, LIGO and Virgo interferometers

detected a GW signal from a *double neutron star* (DNS) merger: this event was named GW170817 (see Abbott et al. [3]). Until today a *black hole neutron star* (BHNS) binary system has not been observed but a BHNS merger candidate, named S190426c , has been detected on April 26, 2019 (see Lattimer [4]). The third observation run by LIGO and Virgo started on April 1, 2019 and is expected to end on April 30, 2020[1].

Event	$m_1\ (M_\odot)$	$m_2\ (M_\odot)$	$M_{fin}\ (M_\odot)$	$d_L\ (Mpc)$	z
GW150914	$35.6^{+4.7}_{-3.1}$	$30.6^{+3.0}_{-4.4}$	$63.1^{+3.4}_{-3.0}$	440^{+150}_{-170}	$0.09^{+0.03}_{-0.03}$
GW151012	$23.2^{+14.9}_{-5.5}$	$13.6^{+4.1}_{-4.8}$	$35.6^{+10.8}_{-3.8}$	1080^{+550}_{-490}	$0.21^{+0.09}_{-0.09}$
GW151226	$13.7^{+8.8}_{-3.2}$	$7.7^{+2.2}_{-2.5}$	$20.5^{+6.4}_{-1.5}$	450^{+180}_{-190}	$0.09^{+0.04}_{-0.04}$
GW170104	$30.8^{+7.3}_{-5.6}$	$20.0^{+4.9}_{-4.6}$	$48.9^{+5.1}_{-4.0}$	990^{+440}_{-430}	$0.20^{+0.08}_{-0.08}$
GW170608	$11.0^{+5.5}_{-1.7}$	$7.6^{+1.4}_{-2.2}$	$17.8^{+3.4}_{-0.7}$	320^{+120}_{-110}	$0.07^{+0.02}_{-0.02}$
GW170729	$50.2^{+16.2}_{-10.2}$	$34.0^{+9.1}_{-10.1}$	$79.5^{+14.7}_{-10.2}$	2840^{+1400}_{-1360}	$0.49^{+0.19}_{-0.21}$
GW170809	$35.0^{+8.3}_{-5.9}$	$23.8^{+5.1}_{-5.2}$	$56.3^{+5.2}_{-3.8}$	1030^{+320}_{-390}	$0.20^{+0.05}_{-0.07}$
GW170814	$30.6^{+5.6}_{-3.0}$	$25.2^{+2.8}_{-4.0}$	$53.2^{+3.2}_{-2.4}$	600^{+150}_{-220}	$0.12^{+0.03}_{-0.04}$
GW170817	$1.46^{+0.12}_{-0.10}$	$1.27^{+0.09}_{-0.09}$	≤ 2.8	40^{+7}_{-15}	$0.01^{+0.00}_{-0.00}$
GW170818	$35.4^{+7.5}_{-4.7}$	$26.7^{+4.3}_{-5.2}$	$59.4^{+4.9}_{-3.8}$	1060^{+420}_{-380}	$0.21^{+0.07}_{-0.07}$
GW170823	$39.5^{+11.2}_{-6.7}$	$29.0^{+6.7}_{-7.8}$	$65.4^{+10.1}_{-7.4}$	1940^{+970}_{-900}	$0.35^{+0.15}_{-0.15}$

Table 1: Main observed properties of published GW detection, taken from Abbott et al. [2]. m_1: mass of the primary object; m_2: mass of the secondary object; M_{fin}: mass of the final object; d_L: luminosity distance; z: redshift. For all properties, median values with 90% credible intervals. All the events are double BH mergers except GW170817, which is a double NS merger.

[1]From `https://www.ligo.caltech.edu/`

All the detected GW events, displayed in Table 1, are caused by the *coalescence*, i.e. the process by which two objects merge to form a single object, between the compact members of a binary system. The study of formation and evolution of such compact objects binary systems, i.e. BHB, DNS and BHNS binaries, is crucial to understand the astrophysics of GW.

In this regard, GW150914 taught several revolutionary concepts about BHs. First we confirmed not only the existence of BHB, which has been predicted a long time ago, but also that such binary systems are able to merge within a Hubble time. Furthermore eight of the ten merging BHB detected so far feature BHs with mass greater than 20 $M_{\odot}$. As opposed to the discovery of BHB, which were expected to exist, the detection of these massive stellar BHs was a surprise for the astrophysical community, because the few measures of the dynamical mass of stellar BHs are smaller than $20\,M_{\odot}$. Also the majority of BH theoretical models did not predict the existence of BH with mass $m_{BH} > 30\,M_{\odot}$.

The eleven GW detections provide boundaries for compact binary models, which can be improved through the use of simulations. In this work we analyze the data resulting from two simulations ran with the binary population-synthesis code MOBSE. The analysis focuses on the *delay time* t_{delay}, i.e. the interval of time between the formation of the binary and its merger. The delay time is a fundamental parameter to evaluate the *merger rate*, namely if a binary can merge within a Hubble time, then we are able to observe the merger event. We evaluate the influence over t_{delay} from several parameters: metallicity, natal kick and the type of compact binary (BHB, BHNS and DNS).

This work is divided in two parts: the first is a brief overview of the physical processes that occur during the single star and binary evolution; the second part is a overview of the implementation of these processes into the MOBSE code, then we show the results of our analysis. In Section 2 we discuss the pre-Supernova mass loss through stellar winds, in Section 3 we discuss the different paths that lead to a SN explosion, in Section 4 we show a mass spectrum scenario for the formation of compact remnants, in Section 5 we review the main processes that occur during binary evolution, in Section 6 we present the isolated binary formation scenario, in Section 7 we give an overwiev of the MOBSE code and then in Sections 8 and 9 we show the results of the analysis and the conclusions.

2 Stellar evolution of binary system members

This work focuses on binary systems that form and evolve under the *isolated binary formation scenario*, i.e. the model which describes the formation of merging compact remnants evolved from isolated binaries, which are stellar binary systems which do not interact with other stars or compact objects during their evolution (e.g. Mapelli et al. [5, 6]). An alternative to this model is the *dynamical evolution scenario* which will not be an argument of debate in this work.

As a starting point we consider the evolution of the single stars of the binary, from main sequence up to *supernova* (SN) explosion. Not all stars are expected to leave a compact remnant at the end of their evolution: only massive stars ($M_{star} \gtrsim 8\ M_{\odot}$) leave BHs or NSs as remnants, so we will focus on their evolution path.

2.1 Pre-supernova mass loss

Compact remnants are left by stars at the end of their evolution. The nature and final mass of these remnants depend mainly on the pre-SN mass of the star, which will greatly influence the subsequent SN explosion. In the case of a massive star, the most influential process on stellar evolution is mass loss through large outflows, called *stellar winds*, that gradually remove their envelope.

In massive hot stars, namely O and B type main sequence stars (see Vink, de Koter, and Lamers [7]), blue supergiants (BSG), luminous blue variables (LBV) (see Belczynski et al. [8]) and Wolf-Rayet (WR) stars (see Vink, Jorick, and de Koter [9]), stellar winds are induced by radiation pressure on metal lines. Consequently this radiation driven mass loss depends on metallicity, with the dependence being $\dot{M} \propto Z^{\beta}$, with the value of β depending on different models. However some uncertainties in the theoretical models are present due to *multiple scattering*, i.e. the possibility that a photon interacts more than one time before leaving the atmosphere, and *wind clumping*, i.e. inhomogeneities in the stellar outflow.

In addition to these sources of uncertainty, when evaluating β we have to consider the fact that the metallicity dependence is greatly reduced when the star is close to be radiation pressure dominated ($\Gamma_e \to 1$). For this kind of stars we have to take into account the stellar wind dependence on the electron-scattering Eddington factor $\Gamma_e = \kappa_e\, L/(4\pi\, c\, G\, m)$, where κ_e is the electron scattering opacity coefficient as reported by Chen et al. [10]. The

values of β in relation to Γ_e used in this work are stated in Section 7. Finally, as reviewed in Limongi [11], stellar rotation can influence the pre-SN mass of a star: rotation enhances luminosity, increasing the winds; on the other hand rotation causes chemical mixing, increasing the mass of Helium (He) and Carbon-Oxygen (C-O) cores.

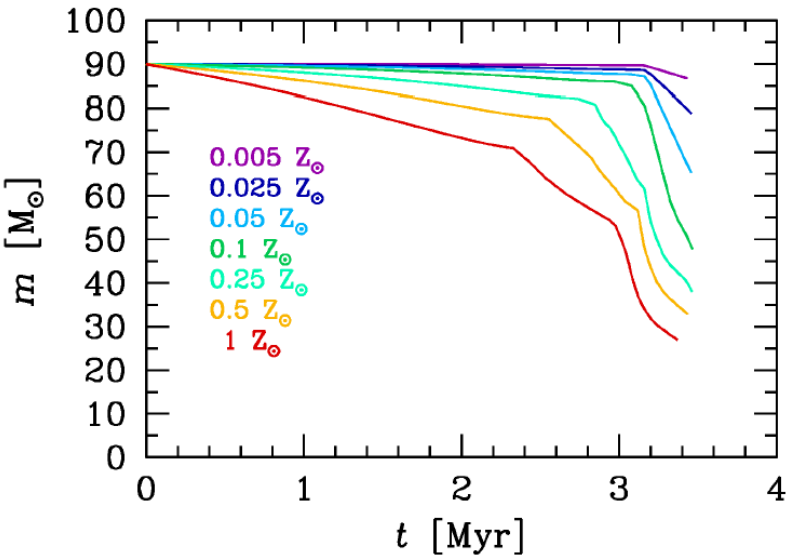

Figure 2: Evolution of stellar mass as a function of time for a star with ZAMS mass $M_{ZAMS} = 90 M_{\odot}$ and seven different metallicities, from $0.005\, Z_{\odot}$ to $Z_{\odot}$, which is assumed as $Z_{\odot} = 0.02$. Image taken from Mapelli [12].

3 Supernova explosions

At the end of the last stable burning cycle, the core of the star is expected to collapse, eventually leading to the ejection of the envelope and to a SN explosion. Unfortunately the causes both of the collapse and of the explosion are still uncertain. Nonetheless a general core collapse scenario is accepted even if some open issues exist within.

In this Section we briefly describe four different core collapse scenarios, namely *electron-capture*, *core-collapse*, *pulsational instability* and *pulsational pair instability* SNe, and their influence on the SN explosion engine.

3.1 Electron-capture supernovae

After He and C burning phases, the lowest mass progenitors develop an Oxygen-Neon-Magnesium core (O-Ne-Mg), but reach *electron degeneracy* before Ne burning can be ignited. Due to low reaction thresholds of Ne and Mg, the increasing electron energy enables *electron captures*, a process in which free electrons are captured by protons producing neutrons and neutrinos ($p + e^- \rightarrow n + \nu$). During this phase of the collapse, called *neutronization*, the rapid drop of the electron degeneracy pressure triggers the gravitational collapse of the core. The collapse ends with the formation of a *proto-neutron star* (PNS). If the consequent SN explosion occurs, the result is an *electron-capture* SN (ECSN). As the collapse unfolds, a very steep density gradient between the O-Ne core and the thin C-O shell around it develops, which is crucial in the explosion phase (see Janka [13] for a review of the explosion mechanisms of core collapse SNe).

Solar metallicity stars in the $9 - 9.25\,M_\odot$ mass range are expected to undergo an ECSN. However the mass range for an ECSN to occur is estimated to shift and widen for low metallicity stars and in binary systems with mass loss or transfer (see Section 5).

3.2 Core-collapse supernovae

After He burning phase, the C-O core undergoes a succession of nuclear burning cycles, the last being Silicon (Si) burning. As Si burning occurs, the remaining Iron (Fe) core, which can not go through an esothermic burning cycle, approaches the Chandrasekhar mass ($M_{Ch} \approx 1.4\,M_\odot$) (see Chandrasekhar [14]). When this limit is reached, the degeneracy pressure of relativistic electrons does not keep the core stable against dynamical collapse.

Then by means of *electron captures* the degeneracy pressure decreases even more, *neutronization* takes place and leads to the formation of a PNS. If the consequent SN explosion occurs, the result is a *core-collapse* SN (CCSN) (see Janka [13]).

In contrast to the ECSN case, the density gradient in the Fe core and the shells around is much flatter, leading to a larger ram pressure of the infalling stellar matter. The density gradient causes CCSN progenitors harder to blow up than ECSN progenitors. In Figure 3 are plotted the density gradients of both ECSN and CCSN progenitors.

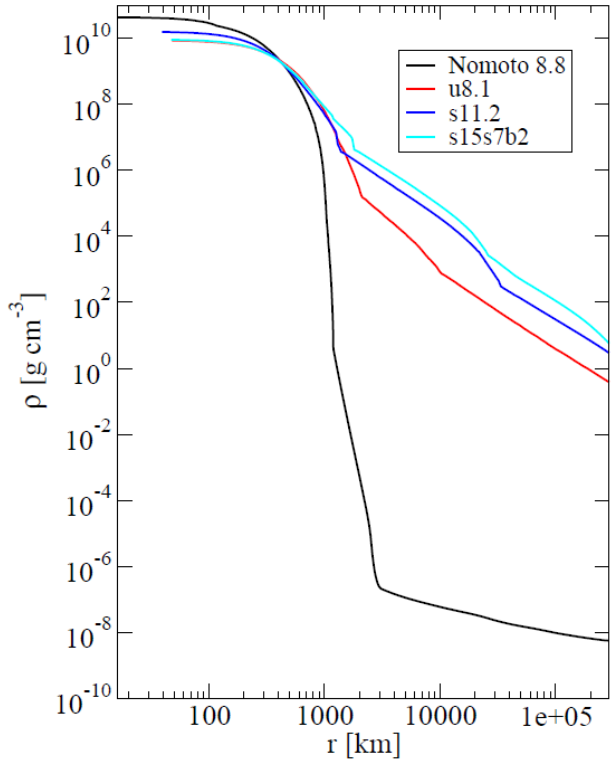

Figure 3: Core-density profiles of different SN progenitors at the onset of gravitational collapse, from Janka [13]. *Black line*: O-Ne-Mg core of a 8.8 $M_\odot$ star. *Red line*: Fe core of a metal poor star (0.0001 $Z_\odot$) with mass 8.1 $M_\odot$. *Blue and cyan lines*: Fe cores of solar metallicity star with respective mass of 11.2 and 15 $M_\odot$.

3.3 Pair-instability supernovae

Some massive stars are expected to undergo *pair instability* (see Fowler and Hoyle [15], Barkat, Rakavy, and Sack [16], and Rakavy and Shaviv [17]) and *pulsational pair instability* SNe (see Woosley [18]). The fundamental process causing these SNe is *electron-positron pair production* ($\gamma \rightarrow e^+ + e^-$), which becomes active if the He core mass M_{He} exceeds $\sim 30\, M_\odot$ and the core temperature is $\gtrsim 7 \times 10^8\, K$. This process has the effect of removing photon pressure from the core and of triggering the collapse before the Fe core has formed. Pair instability SNe occur if $M_{He} > 135\, M_\odot$, the outcome being a direct collapse of the star into a BH. For $64 \leq M_{He} \leq 135\, M_\odot$ the collapse triggers an explosive burning of heavier elements, which have disruptive effects. This leads to a complete disruption of the star, leaving no remnant. Instead for $32 \leq M_{He} \leq 64\, M_\odot$, pulsational pair instability SNe take place: pair production induces pulsations of the core, triggering an enhanced mass loss, leaving at the end a remnant lighter than in the case of direct collapse.

3.4 Supernova explosion engine

The entire dynamical collapse phase, with core radius starting at the order of $\sim 1000\, km$ and ending at the order of $\sim 10\, km$, lasts only $\sim 10\, ms$ releasing an enormous amount of gravitational energy $E_{gr} \approx 5 \times 10^{53}\, erg$. Only a small fraction of this energy is needed to blow out the envelope prompting the SN explosion, but how this gravitational energy can be converted into kinetic energy of the envelope remains an open problem (see Bethe and Wilson [19]).

The most commonly investigated explosion mechanism is the *convective enhanced, neutrino driven SN engine* (e.g. Fryer et al. [20]). This model states that after the formation of the PNS, the collapse is effectively halted by neutron degeneracy pressure. The abrupt collapse stop causes a bounce shock to move outwards from the core. For the SN explosion to occur, the shock wave has to overcome the pressure of the infalling matter from the outer layers of the star.

In the case of ECSN of low mass progenitors, the shock wave may be able to blow the envelope out and trigger the explosion. Owing to the low ram pressure exerted by the outer layers and to the very steep density gradient at the edge of the O-Ne-Mg core, the accretion shock continues to grow, thus creating ideal conditions for neutrino energy transfer. Consequently a matter outflow develops, which causes the explosion (Janka [13]).

In the CCSN case, as the shock wave moves through the envelope, neutrino loss reduces its energy, effectively stalling it. The SN explosion happens only if the shock can be revived by some mechanism, which in this scenario is the formation of a non-radial convective instability region between the PNS surface and the shock stalling radius (e.g. a Rayleigh-Taylor instability). These kinds of instabilities can convert the leaking energy from the diffusing neutrinos into kinetic energy by pushing outward the convective region (Figure 4). If the kinetic energy of the convective region overcomes the ram pressure of the infalling stellar matter, then the SN explosion takes place. If this is not the case, the SN fails.

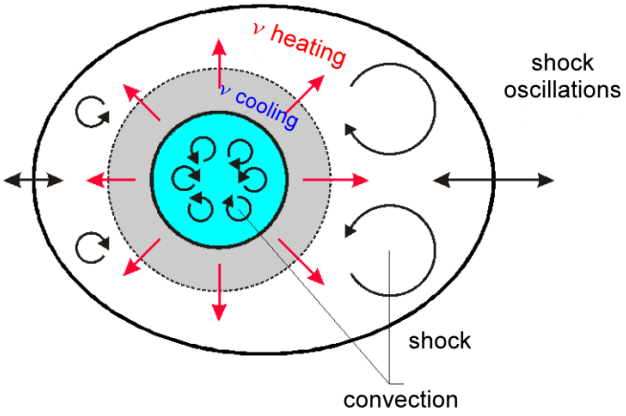

Figure 4: Cartoon of the crucial elements of the neutrino-driven SN engine, from Müller [21]. Neutrinos are emitted from the accretion layer (grey) around the PNS (cyan) and from its core. A fraction of the neutrinos are reabsorbed in the layer behind the shock. In this region, non-spherical flow can develop because neutrino heating drives convective overturn and because of an acoustic instability of the shock.

All that said, we should have all the ingredients to simulate consistently a SN explosion under the convective scenario, however 2-D and 3-D simulations are too challenging to compute for a large number of stars. Thus, to study the mass distribution of compact remnants, SN explosions are artificially induced by injecting in the pre-SN model some amount of kinetic energy or thermal energy at an arbitrary mass location. Then the evolution of the shock is computed through 1-D hydrodynamical simulations with a simplified model for neutrinos. In this way the evolution a large numbers of

stars can be simulated.

To complete this model a criterion for the success of the SN is required. In this work we adopt the simplest approach proposed in Fryer et al. [20]: a criterion based on the pre-SN C-O core mass M_{CO} and on the total final mass of the star M_{fin}. We assume that M_{CO} determines the occurrence of a core-collapse SN or a direct collapse to a BH (if $M_{CO} \gtrsim 7.6\, M_{\odot}$), while M_{fin} determines the entity of *fallback*, i.e. the amount of the infalling stellar matter on the PNS.

Even if this approach is quite simplified, we can refer to more refined models to verify its goodness. To predict the success of a SN explosion, O'Connor and Ott [22] offer a criterion based on the *compactness parameter* of the star ξ_m:

$$\xi_m = \frac{m/M_{\odot}}{R(m)/1000\, km}, \tag{1}$$

where $R(m)$ is the radius which encloses a given mass m. Usually the compactness is defined for $m = 2.5 M_{\odot}$ ($\xi_{2.5}$) and is measured at core bounce. The simulations made with this model show that the larger $\xi_{2.5}$ is, the shorter the time to form a BH, meaning that stars with a larger value of $\xi_{2.5}$ are more likely to collapse into a BH without a SN explosion. Limongi [11] found a strong correlation between M_{CO} and the compactness of the PNS at the beginning of collapse $\xi_{2.5}$. This model also predicts a non-monotonic behaviour of SN explosions with the stellar mass, the *islands of explodability* scenario, i.e. ranges of mass where the star is expected to explode surrounded by other mass ranges where the star dies with a direct collapse.

The criterion proposed by O'Connor and Ott [22] is not implemented in the MOBSE code (see Section 7) because it depends on the $\xi_{2.5}$ parameter, which has to be evaluated at the beginning of the core collapse and would require a stellar evolution model which integrates a massive star until a Fe core is formed. This is prohibitive for most stellar evolution models. Nevertheless we can take into consideration the results in Limongi [11] to assume that the simplified model used in this work can effectively describe the overall trend of a collapsing star.

Another physical ingredient that impacts on the outcome of a core-collapse SN is the time to launch the shock τ_{shock}. If the explosion occurs more than $\sim 250\, ms$ after the bounce (*delayed* SN explosion), then the peak energy will be greatly reduced compared to the case when the explosion oc-

curs before the 250 ms threshold (*rapid* SN explosion) (refer to Fryer et al. [20]).

To summarize briefly, the model we used to describe the general framework of a collapsing star depends on three parameters: M_{CO}, M_{fin} and τ_{shock}.

4 Compact remnants

Despite several uncertainties (coming from stellar winds and SN explosions) that make difficult to model a mass spectrum of compact remnants, if we make some assumptions for simplicity, we can deduce a general idea.

As stated before, stellar winds, thus metallicity, have a large influence on the compact remnant mass (see Heger et al. [23]). In the case of a solar metallicity star ($Z_\odot \approx 0.02$), a large fraction of its mass is removed due to the extremely efficient stellar winds, and the final mass of the star M_{fin} is lower than the initial one. The mass of compact remnants is also lower than M_{fin}, because with solar metallicity a core collapse SN always occurs. Both these effects, along with the *islands of explodability* scenario, can be seen in Figure 5.

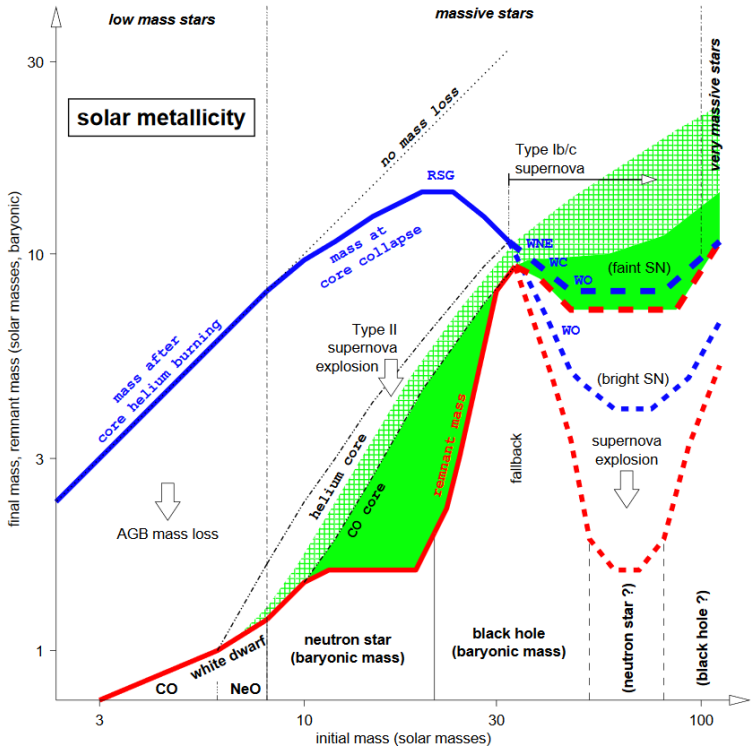

Figure 5: Final mass of a star (M_{fin}) in blue and mass of the remnant ($M_{remnant}$) as a function of the ZAMS mass of the star (M_{ZAMS}). $Z = Z_\odot$. Image from Heger et al. [23].

Instead in the case of a metal-free star stellar winds are much weaker than the previous instance, resulting in the loss of a negligible fraction of mass as we can see in Figure 6.

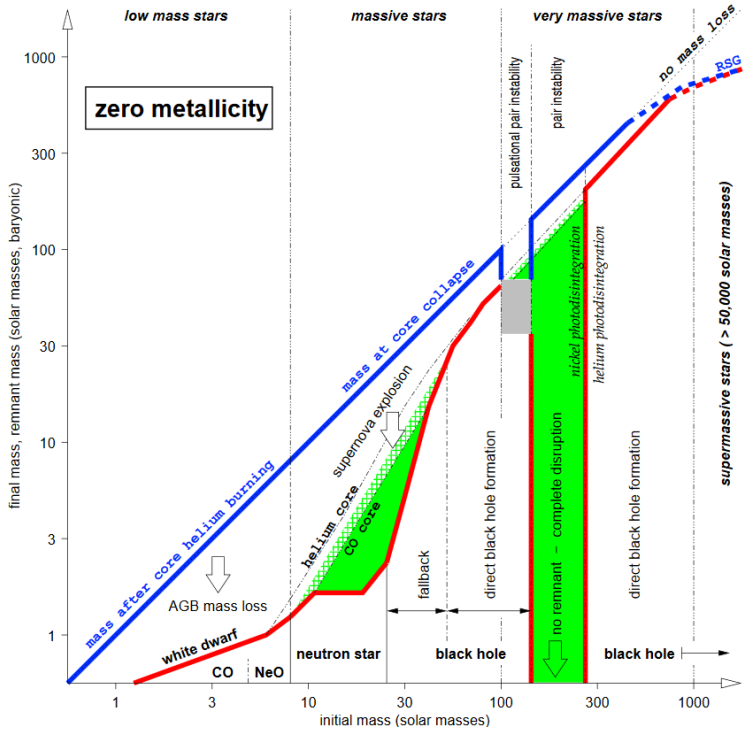

Figure 6: Final mass of a star (M_{fin}) in blue and mass of the remnant ($M_{remnant}$) as a function of ZAMS mass of the star. $Z = 0$. Image from Heger et al. [23].

The mass of compact remnants follows two different scenarios: for $Z = 0$ and below a given ZAMS limit mass ($M_{\mathsf{ZAMS}} \sim 30 - 40\ M_{\odot}$) the SN takes place in any case and the compact remnant mass is relatively small; above the limit mass the SN fails and the star directly collapses to a BH, whose mass is larger than in the occurrence of a SN explosion. Unfortunately what happens at intermediate metallicity between zero and solar remains an open issue.

We can now describe a general mass prediction scenario (as in Fryer et al. [20] and Spera, Mapelli, and Bressan [24]) for compact remnants using the *zero-age main sequence* mass of a star M_{ZAMS} as the main parameter:

- If M_{ZAMS} is relatively low ($7-30\,M_{\odot}$), then stellar winds are not very effective in removing mass (with the exception of super *asymptotic giant branch* stars) regardless of the metallicity. In this case the details of the SN explosion, as the energy of the explosion and entity of fallback, are fundamental to determine the final mass of the remnant.

- If $30 \lesssim M_{\mathsf{ZAMS}} \lesssim 60\,M_{\odot}$, then the efficiency of stellar winds in removing mass is critical to determine the mass of the compact remnant. In the condition of low metallicity ($Z \lesssim 0.1\,Z_{\odot}$) and low Eddington factor ($\Gamma_e < 0.6$) stellar wind mass loss is not particularly large. Thus, the Carbon-Oxygen mass M_{CO} and the final mass M_{fin} may be large enough to avoid a core-collapse SN explosion. Then the star may collapse directly to a BH ($M_{\mathsf{BH}} \gtrsim 20\,M_{\odot}$), unless a pair instability or pulsational pair instability SN occurs. On the other hand in case of high metallicity ($\sim Z_{\odot}$) or large Eddington factor ($\Gamma_e > 0.6$) stellar wind mass loss is greatly effective and may cause small M_{CO} and M_{fin}. The star is supposed to undergo a CCSN explosion and to leave a relatively small remnant.

- If $60 \lesssim M_{\mathsf{ZAMS}} \lesssim 110\,M_{\odot}$ and metallicity is very low ($Z < 0.001\,Z_{\odot}$), a pulsational pair instability SN takes place, enhancing mass loss and resulting in a reduced BH final mass ($M_{\mathsf{BH}} \sim 30-55\,M_{\odot}$) than expected from the case of direct collapse ($M_{\mathsf{BH}} \sim 50-100\,M_{\odot}$).

- If $110 \lesssim M_{\mathsf{ZAMS}} \lesssim 230\,M_{\odot}$ and the condition of very low metallicity is satisfied ($Z < 0.001\,Z_{\odot}$), the star enters the pair instability SN regime, leading to its complete disruption thus leaving no remnant.

- If the star is very massive ($M_{\mathsf{ZAMS}} > 230\,M_{\odot}$) and $Z < 0.001\,Z_{\odot}$, it is able to collapse directly into an intermediate-mass BH ($M_{\mathsf{BH}} \gtrsim 100\,M_{\odot}$).

The occurrence of both pair instability and pulsational pair instability SNe causes a *BH mass gap* in the mass spectrum, between $M_{\mathsf{BH}} \sim 60\,M_{\odot}$ and $M_{\mathsf{BH}} \sim 120\,M_{\odot}$ as seen in Figure 7.

This model of the mass spectrum of compact remnants of stars with low metallicity, with all the features aforementioned in Sections 3.2 and 3.3, is summarized in Table 2.

M_{ZAMS}	Process	Remnant	$M_{remnant}$
8 - 30 $M_\odot$	core collapse SN	NS	1.4 - 3 $M_\odot$
30 - 60 $M_\odot$	core collapse SN	BH	$\sim 20\, M_\odot$
60 - 110 $M_\odot$	puls. pair instability	BH	30 - 55 $M_\odot$
110 - 230 $M_\odot$	pair instability	No remnant	None
$> 230\, M_\odot$	direct collapse	BH	$> 100\, M_\odot$

Table 2: Mass spectrum of compact remnants (low metallicity).

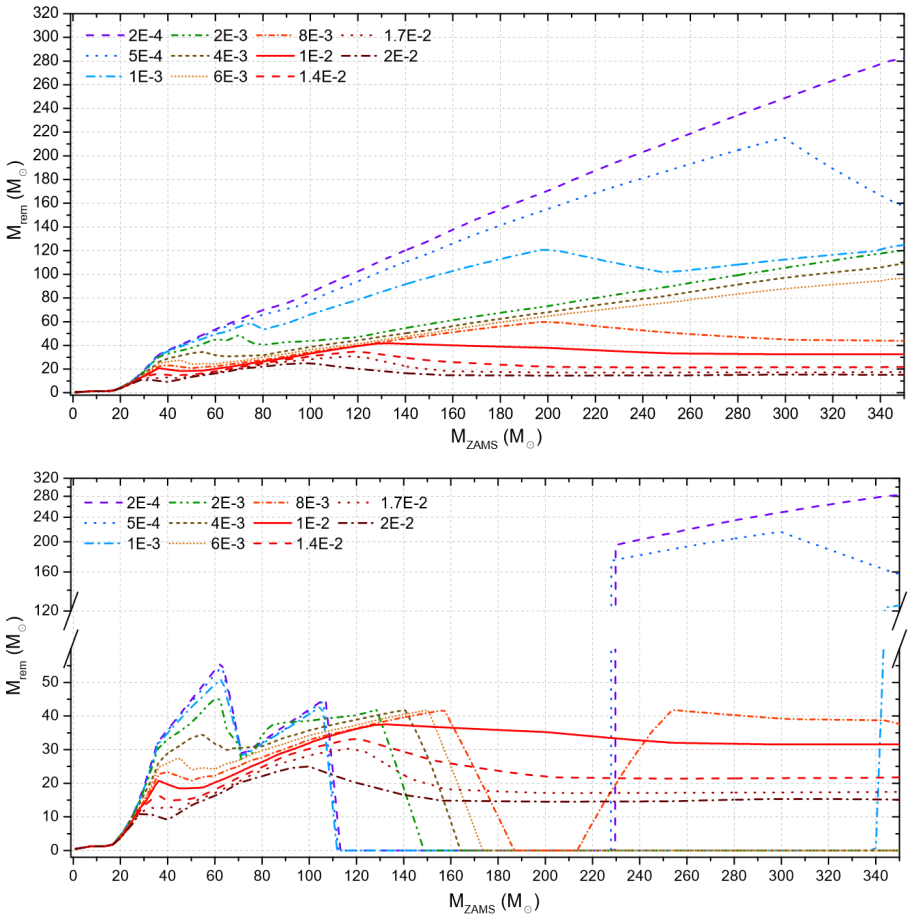

Figure 7: Mass of the compact remnant ($m_{remnant}$) as a function of the ZAMS mass of the star (M_{ZAMS}). The dotted or dashed lines of different colours refer to different metallicities (in $Z_{\odot}$ with the legend in the upper left corners of both panels. In both panels has been used a *delayed* core collapse SN mechanism, described in Section 3.2. *Top*: simulations ran taking into account only ECSN and CCSN. *Bottom*: pulsational pair-instability and pair-instability SNe have been included in the simulations; the BH mass gap is noticeable between $M_{\mathsf{BH}} \sim 60\, M_{\odot}$ and $M_{\mathsf{BH}} \sim 120\, M_{\odot}$. This figure was taken from Spera and Mapelli [25].

4.1 Natal kicks

Following the SN explosion, compact remnants receive a *natal kick*, i.e. recoil velocity, owing to the presence of anisotropy both in mass loss and in neutrino flux, the former more important than the latter, and to momentum conservation (see Janka [13] for a review).

In the instance of direct collapse of the star, most studies assume that BHs formed through such a process receive no kick. Natal kicks have a determinant effect on the evolution of a compact remnant binary system: depending on their energy they may either unbind the binary or change its orbital properties; they also have remarkable consequences on the merger rate and on the properties (e.g. spin and mass distribution) of merging compact objects. However, not only it is extremely difficult to give an estimate of natal kicks from SN simulations, but measurements of natal kicks are scarce as well, even scarcer for BHs.

Indirect observations of NS natal kick give conflicting results: a possible explanation resides in the dependence of the natal kick on the regime of SN explosion (e.g. ECSN or CCSN, see Giacobbo and Mapelli [26]) or on the binarity of the NS progenitor (e.g close or detached binary). If the NS progenitor evolves in a *close* binary system (a system where an exchange of mass between the two stars has taken place, see Section 5.1) it may be heavily stripped by mass transfer to its companion, causing the star to undergo an *ultra-stripped* SN explosion. In this process the ejected mass is relatively small ($\lesssim 0.1 M_{\odot}$) and the consequent natal kick is low ($\lesssim 50 km/s$) (see [94]).

Furthermore, Hobbs et al. [27] found that the distribution of velocities of 233 single pulsars in the Milky Way is well described by a Maxwellian distribution with 1-D root-mean-square $\sigma_{\mathsf{CCSN}} = 265\ km/s$. As said in Section 7, this value is used in the MOBSE code.

Concerning BH natal kicks, unfortunately only few indirect measurements (coming from BHs in X-ray binaries, see Mirabel [28]) give us insight on the nature and the intensity of these kicks. Most models, like in Fryer et al. [20], assume that the natal kicks of BHs are drawn from the same distribution as NS kicks, but reduced by some factor as in

$$v_{\mathsf{BH}} = \frac{M_{\mathsf{NS}}}{M_{\mathsf{BH}}}\, v_{\mathsf{NS}}\ , \tag{2}$$

where v_{BH} is the natal kick of a BH with mass M_{BH} and v_{NS} is the natal kick of a NS with mass M_{NS}.

Another approach to this problem is that of reducing the natal kick by the amount of fallback, under the hypothesis that fallback quenches the initial asymmetries, as in

$$v_{\mathsf{BH}} = (1 - f_{fb})\, v_{\mathsf{NS}} \,, \tag{3}$$

where f_{fb} measures the intensity of the fallback ($f_{fb} = 0$ for no fallback and $f_{fb} = 1$ for direct collapse).

5 Evolution of isolated binaries

Now that we have the evolution framework of a massive star, from main sequence to SN explosion and its consequences, how does a compact object binary system form? If the binary system is sufficiently wide (i.e. a *detached binary*), then both of its stars will undergo the entire evolution process separately, barely influencing each other. After both stars have come to the end of their evolution, a compact remnant binary will be left. In the other instance, if the binary is close enough (i.e. a *close binary*), it will go through a different evolution path: the stars will influence each other during their entire life.

In this Section we will briefly describe some of the most important *binary evolution processes* that take place in this case, namely stellar wind mass transfer, *Roche lobe* filling and *common envelope* (CE).

5.1 Mass transfer

Mass transfer between two close stars occurs if the two exchange matter to each other. A mass transfer event can occur under different regimes: by stellar wind or by *Roche lobe* filling.

Whenever a massive star loses mass by stellar wind, its companion may be able to capture some of this mass. The efficiency of this process depends on the amount of lost mass and on the relative wind velocity with respect to the companion star. A description of the *mass accretion rate* by stellar wind (see Hurley, Tout, and Pols [29]) is

$$\dot{M}_2 = \frac{1}{\sqrt{1-e^2}} \left(\frac{G\,M_2}{v_w^2}\right)^2 \frac{\alpha_w}{2a^2} \frac{1}{[1+(v_{orb}/v_w)^2]^{3/2}} \dot{M}_1 \,, \tag{4}$$

where M_2 and $\dot{M}_2$ are respectively the mass of the accreting star and its mass accretion rate, e is the binary eccentricity, G is the gravitational constant, v_w is the velocity of the wind, $\alpha_w \sim 3/2$ is an efficiency constant, a is the semi-major axis of the binary, $v_{orb} = \sqrt{G(M_1+M_2)/a}$ is the orbital velocity of the binary, M_1 and $\dot{M}_1$ are respectively the mass of the donor and its mass loss rate. This kind of mass transfer is rather inefficient.

Mass transfer by Roche lobe filling is usually more efficient. The *Roche lobe* of a star in a binary system is the maximum equipotential surface surrounding the star in which all the matter is bound to that star, as pictured in

Figure 8[2]. While its exact shape should be calculated numerically, Eggleton [30] gives a widely used approximation formula:

$$r_{\mathrm{L},1} = a\,\frac{0.49\,q^{2/3}}{0.6\,q^{2/3} + \ln(1+q^{1/3})}\,, \tag{5}$$

where $r_{\mathrm{L},1}$ is the radius of the Roche lobe of star with mass M_1, a is the semi-major axis of the binary, $q = M_1/M_2$ (M_1 and M_2 being the masses of the stars of the binary).

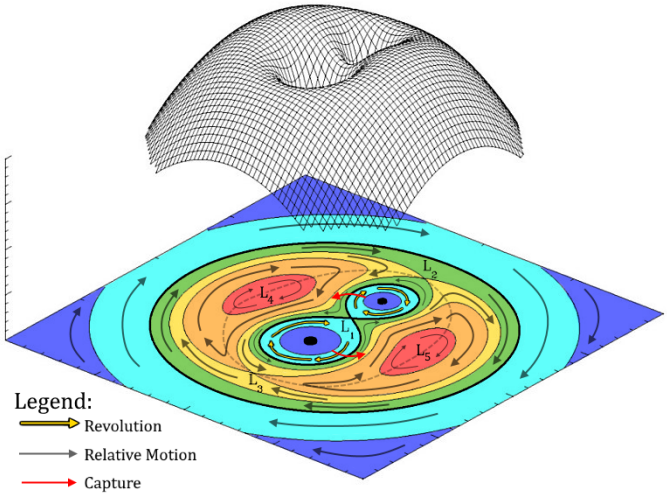

Figure 8: 3-D plot of the Roche potential in a binary system with $m_2 = 2\,m_1$. L_1, L_2 and L_3 are the Lagrangian points of the system. The cyan figures around both the binary members are the Roche lobes, which are connected in L_1.

In a binary system, Roche lobes of the two stars are connected by the L_1 Lagrangian point. Since these are equipotential surfaces, matter that finds itself at or beyond the Roche lobe can flow freely from one star to the other. The roles of the stars taking part in this process are so defined: a star *overfills* (resp. *underfills*) its Roche lobe when its radius is larger (smaller) than the lobe one, such a star is called *donor* (*accretor*). Hence the matter flows from the donor to its companion accretor.

Mass transfer entails several consequences: the first one is obviously a change in the masses of both star, thus influencing the mass of the com-

[2]Colorized version of the image taken from `http://hemel.waarnemen.com/Informatie/Sterren/hoofdstuk6.html`

pact remnant; in the case of a non conservative mass transfer (which is the most realistic case in either of mass transfer regimes), another outcome is the variation on the orbital properties of the binary, leading to an angular momentum variation and thus affecting the semi-major axis.

To fully describe Roche lobe overfilling we need to take into account its stability and on which timescale. A commonly used approach (see Portegies Zwart and Verbunt [31], Hurley, Tout, and Pols [29], and Tout et al. [32]) consists in comparing the following quantities:

$$\zeta_{ad} = \left(\frac{d\ln R_1}{d\ln M_1}\right)_{ad}, \quad \zeta_{th} = \left(\frac{d\ln R_1}{d\ln M_1}\right)_{th}, \quad \zeta_{\mathsf{L}} = \left(\frac{d\ln r_{\mathsf{L},1}}{d\ln M_1}\right), \tag{6}$$

where ζ_{ad} is the change of the radius of the donor needed to adiabatically stabilize the star into a new hydrostatic equilibrium, ζ_{th} is the change of the radius of the donor needed to stabilize the star into a new thermal equilibrium, ζ_{L} is the change of the Roche lobe of the donor. All changes of radius are induced by mass loss.

The comparison of these radius changes quantities distinguishes three regimes of mass transfer stability:

- If $\zeta_{\mathsf{L}} > \zeta_{ad}$, then the star expands faster than its Roche lobe and mass transfer is unstable over a *dynamical* timescale.
- If $\zeta_{ad} > \zeta_{\mathsf{L}} > \zeta_{th}$, then mass transfer is unstable over a *thermal* (Kelvin-Helmhotz) timescale.
- If $\min(\zeta_{ad}, \zeta_{th}) > \zeta_{\mathsf{L}}$, then mass transfer is stable until some other process causes a further change of the radius.

Whether mass transfer is dynamically unstable ($\zeta_{\mathsf{L}} > \zeta_{ad}$) or both stars overfill their Roche lobe, then the binary is expected to merge (if the donor lacks a steep density gradient between core and envelope), or to enter CE, in the occurrence of a clear separation between the core and the envelope of the donor.

5.2 Common envelope

When the binary system enters CE, the envelope stops corotating with the cores, enclosing both of them. The two stellar cores (or a compact object and a core if the binary is already *single degenerate*) begin a spiral-in motion, due to the friction exerted by the envelope. While spiralling in, the cores

lose orbital energy as an outcome of the gas drag, converting it into heating of the envelope. Consequently the CE expands and becomes more loosely bound. As an effect of this loss of energy, the two objects may undergo a merger inside the CE.

Depending on the efficiency of the ejection, the CE phase has different outcomes: if the envelope is heated enough to be all ejected before the orbiting cores merger, then the resulting post-CE binary is composed of two burning stellar cores (or a core and a compact remnant); additionally the orbital separation of the two objects (whether cores or remnants) is substantially smaller than the initial one. On the other case a single object is formed if the envelope is not ejected rapidly enough to prevent the merger. The occurrence of complete expulsion of the envelope is decisive for fate of a double BH binary: after CE evolution the resulting system has a semi-major axis way shorter than it of its progenitor, making it able to merge within a Hubble time emitting GW.

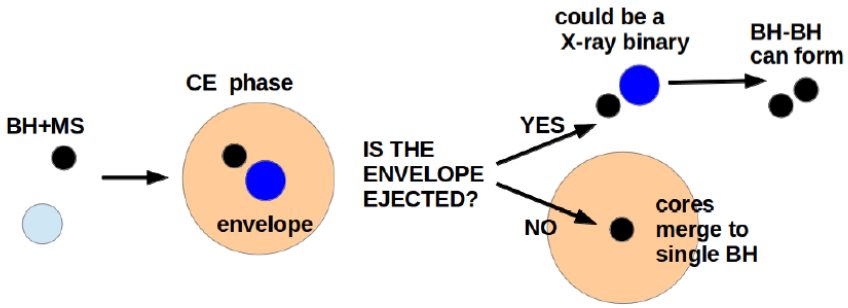

Figure 9: Cartoon of the steps of the CE evolution of a BH binary, taken from Mapelli [12]. The BH is rendered as a black circle, while its main sequence star companion as a cyan circle. As the companion star evolves, the radius of its envelope increases until the binary enters the CE phase. The envelope and the naked He core are rendered respectively in orange and blue.

The most commonly used formalism used to describe a CE is the $\alpha\lambda$ formalism shown in Webbink [33]. The idea behind it is that all the energy used to expel the envelope only comes from the loss of orbital energy of the cores during the spiral in motion. The fraction of orbital energy used to

unbind the envelope (ΔE) can be expressed as

$$\Delta E = \alpha \left(E_{b,f} - E_{b,i}\right) = \alpha \, \frac{G \, M_{c,1} \, M_{c,2}}{2} \, \left(\frac{1}{a_f} - \frac{1}{a_i}\right) , \tag{7}$$

where $E_{b,f}$, a_f and $E_{b,i}$, a_i are respectively the final (after CE phase) and initial (before CE phase) orbital binding energy and semi-major axis of the binary, $M_{c,1}$ and $M_{c,2}$ are the masses of the two cores and α is the dimensionless parameter that quantifies which fraction of the orbital energy is transferred to the envelope.

The binding energy of the envelope is:

$$E_{env} = \frac{G}{\lambda} \, \left(\frac{m_{env,1} \, M_1}{R_1} + \frac{m_{env,2} \, M_2}{R_2}\right) , \tag{8}$$

where M_1 and M_2 are the masses of the members of the binary, R_1, $m_{env,1}$ and R_2, $m_{env,2}$ are their respective radii and envelope masses and λ is the parameter measuring the concentration of the envelope (the smaller λ, the more concentrated the envelope).

The final goal is to derive the final value of the semi-major axis a_f for which the envelope is expelled, that is achieved by imposing $\Delta E = E_{env}$:

$$\frac{1}{a_f} = \frac{1}{\alpha\lambda} \, \frac{2}{M_{c,1} \, M_{c,2}} \, \left(\frac{m_{env,1} \, M_1}{R_1} + \frac{m_{env,2} \, M_2}{R_2}\right) + \frac{1}{a_i} \, . \tag{9}$$

The occurrence of the merger can be evaluated by comparing a_f with the radii of the two cores R_1 and R_2: if $a_f < R_1 + R_2$, then the binary will merge during CE phase; otherwise the system remains binary after the end of CE phase. Equation 9 depends on the $\alpha\lambda$ parameter, meaning that the larger (resp. smaller) $\alpha\lambda$, the larger (smaller) the final orbital separation.

However the simplicity of this model comes at a cost, namely it has been known for a long time that this model offers a poor description of the physics of CE phase, which is considerably more complicated (see Ivanova et al. [34]). It would be extremely important to model the CE in detail, unfortunately simulating numerically such a system is prohibitive for current simulations. Therefore we have to persist in using the $\alpha\lambda$ model and attempt to improve it. While there are ways to remove the λ parameter, as estimating E_{env} directly from stellar models, this formalism is dependent on α anyway, as shown in Xu and Li [35]. This dependence is an open issue due to the existence of a number of observed systems that require $\alpha > 1$, which is obviously non-physical. Nonetheless these kind of values are needed by the *binary population-synthesis codes* to run according to the observations, for this reason the simulations analyzed in this work use $\alpha = 5$ (see Section 7).

6 Isolated binary formation scenario

In Sections 2, 3, 4 and 5 we provided an overview of the main processes occurring during the *isolated binary formation scenario*, which is only one of many existing models of binary evolution. We can now put together all the steps previously presented to effectively summarize the path that leads to a BHB (or a compact object binary) (see Mapelli et al. [5, 6]).

The starting point is a binary system in which its members are both massive stars ($M_{\mathsf{ZAMS}} \gtrsim 8\,M_{\odot}$), gravitationally bound since their birth. We call the more massive star between the two *primary*, the other *secondary*. After the primary star has undergone core Hydrogen (H) burning, it exits the main sequence, increasing its radius and becoming a giant star. The large expansion of the star causes its envelope to exceed its Roche lobe, triggering an episode of mass transfer to the secondary star. Following the end of the H shell burning phase, if the He core is large enough ($M_{He} > 135\,M_{\odot}$, which requires $M_{\mathsf{ZAMS}} > 230\,M_{\odot}$), then collapses directly to an intermediate mass BH. On the other hand if the star undergoes one of the several types of SN explosion, it leaves a smaller BH, which received a natal kick from the parent explosion. However a direct collapse is preferred because it leads to a more massive BH. At this stage the binary radius is still rather large, much larger than it is required for a BHB to merge.

At the same time of the rapid evolution (few Myr for a star with $M_{\mathsf{ZAMS}} \gtrsim 30\,M_{\odot}$) of the primary star, the secondary remains in the main sequence, until it ends the core H burning phase. As the primary did, while the H shell burning phase takes place, it increases its radius and expands its envelope; then, due to the smaller binary radius, the system enters the CE phase and the cores start spiralling in. In case of ejection of the CE before the merger occurs, the binary is formed by a BH and a naked He core (i.e. a WR star) with a separation in the order of $\sim 10\,R_{\odot}$, much smaller than the pre-CE one. If the WR star undergoes a core collapse SN explosion (or in the better case a direct collapse) and the system is not unbound by the consequent natal kick, the resulting system is a BHB able to merge within a Hubble time due to its low separation.

The occurrence of the entire scenario is led by two critical quantities: the initial stellar masses M_{ZAMS} and the initial separation between the members of the binary. Concerning the effects of initial separation, if too short, then the stars merge before they can form a BHB; if too large, then the resulting BHB will be never be able to merge. Instead the separation has to be large enough to allow the binary to enter CE and then to live a close BHB. The

range of initial orbital separations depends on CE efficiency and on details of stellar mass and radius evolution.

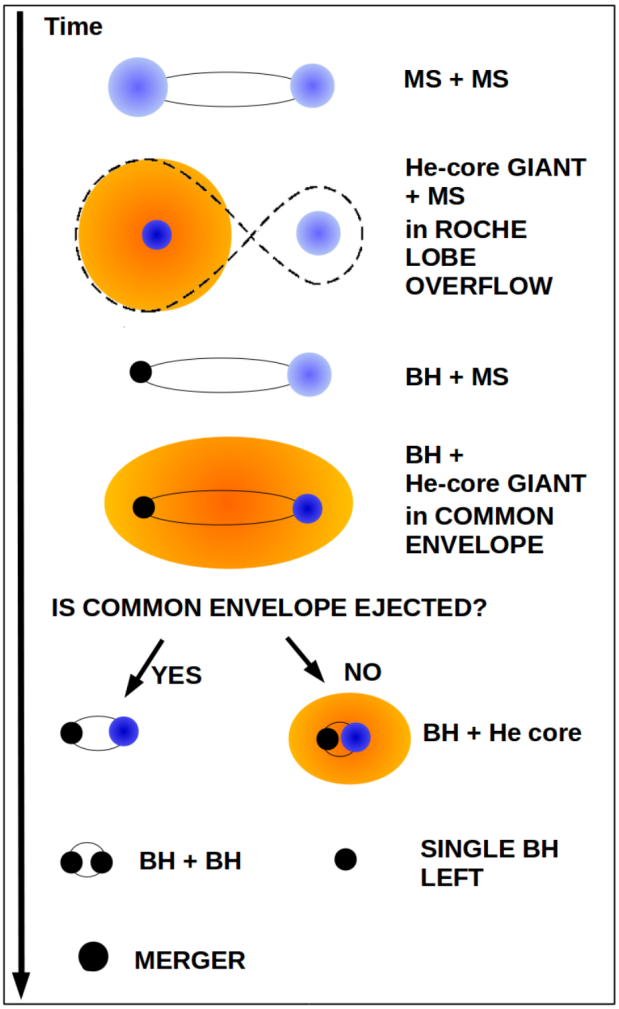

Figure 10: Cartoon of the evolution of a binary system under the isolated binary scenario. Image taken from Mapelli [12].

7 MOBSE and simulations

The data analyzed in this paper come from simulations ran with the MOBSE code. MOBSE, which stands for *Massive Objects in Binary Stellar Evolution*, is an updated version of the BSE binary population-synthesis code (see Hurley, Tout, and Pols [29]). A *binary population-synthesis code* is a Monte-Carlo based code which combines a description of stellar evolution with prescriptions for SN explosions and with a formalism for binary evolution processes. For a detailed description of MOBSE, see Giacobbo, Spera, and Mapelli [36] and Mapelli et al. [5]. In this section we will briefly summarize the main features of MOBSE, referring to Giacobbo and Mapelli [37].

7.1 Pre-SN mass loss and SN explosions

In MOBSE the treatment of stellar winds for hot massive stars is based on Vink, de Koter, and Lamers [7] for O and B type stars, on Vink, Jorick, and de Koter [9] for Wolf-Rayet stars and on Belczynski et al. [8] for luminous blue variables. As said in Section 2.1, mass loss is described as $\dot{M} \propto Z^{\beta}$, where Z is the metallicity and β depends on the Eddington factor Γ_e as shown in Table 3.

Value of β	Eddington factor
0.85	$\Gamma_e < 2/3$
2.45 - 2.4	$2/3 \leq \Gamma_e < 1$
0.05	$\Gamma_e \geq 1$

Table 3: Values of β for mass loss depending on Γ_e.

As seen in Section 3, different models exist for different types of SN explosions. MOBSE includes the models of pulsational pair instability and pair instability SN, as well as of two new prescriptions for Fe core collapse SNe: the delayed and the rapid models. In this work only the rapid core collapse SN mechanism is considered, because it allows to reproduce the mass gap of compact objects between ~ 2 and $\sim 5\, M_{\odot}$. A treatment for

both electron capture SNe and accretion-induced white dwarf collapse is also present: in these two cases the final remnant is a NS, resulting from thermonuclear runaway caused by the collapse of the degenerate O-Ne core as a consequence of electron capture reactions.

7.2 Natal kicks and binary evolution

In MOBSE the natal kick of a NS is drawn from a Maxwellian velocity distribution

$$f(v,\sigma) = \sqrt{\frac{2}{\pi}}\,\frac{v^2}{\sigma^3}\,\exp\left(-\frac{v^2}{2\sigma^2}\right), \tag{10}$$

where $v \in [0,\ \infty[$ and σ is the one dimentional *root-mean-square* (rms). Depending on the SN explosion mechanism, whether ECSN or CCSN (see Sections 3.1 and 3.2), MOBSE draws the natal kick from two Maxwellian curves with different rms: which are respectively σ_{CCSN} and σ_{ECSN}.

The BH natal kick is derived from the NS one, as seen in Section 4.1, using $v_{\mathsf{BH}} = (1 - f_{fb})\, v_{\mathsf{NS}}$, where v_{BH} is the velocity randomly sampled from the Maxwellian curve.

To describe the CE phase, we adopt the $\alpha\lambda$ formalism presented in Section 5.2. In our simulations, λ depends on the stellar type (i.e. mass and luminosity) to account for the contribution of recombinations, while α is a free parameter: in this work we consider $\alpha = 5$.

7.3 Initial conditions

Finally we present the initial conditions under which the simulations analyzed in this work were ran. For each binary system, the mass of the primary star M_1 is drawn from a Kroupa initial mass function (IMF, see Kroupa [38]):

$$\mathcal{F}(M_1) \propto M_1^{-2.3}\,, \tag{11}$$

where $5 \leq M_1 \leq 150\ M_\odot$. Subsequently the mass ratio between the secondary and the primary member of the binary $q = M_2/M_1$ (with $q \in [0.1, 1]$) is derived, according to Sana et al. [39],

$$\mathcal{F}(q) \propto q^{-0.1}\,. \tag{12}$$

Also from Sana et al. [39] the orbital period P and the eccentricity e are

derived as:

$$F(\mathcal{P}) \propto \mathcal{P}^{-0.1}\ ,\ \ \mathcal{P} = \log_{10}\left(\frac{P}{\mathsf{day}}\right)\ , \tag{13}$$

$$\mathcal{F}(e) \propto e^{-0.42}\,, \tag{14}$$

where $0.15 \leq \mathcal{P} \leq 5.5$ and $0 \leq e < 1$.

We analyze the data resulting from two simulations, named $\alpha 5$ and CC15α5, of which the initial conditions are in Table 4. For each set of simulations we considered 12 sub-sets with different metallicities $Z = 0.0002$, 0.0004, 0.0008, 0.0012, 0.0016, 0.002, 0.004, 0.006, 0.008, 0.012, 0.016 and 0.02 $Z_{\odot}$. In each sub-set, we simulated 107 binary systems. Thus, each set of simulations is composed of 1.2×10^8 compact objects binaries.

ID	σ_{ECSN}	σ_{CCSN}	SN	α
$\alpha 5$	15.0 km/s	265.0 km/s	rapid	5.0
CC15α5	15.0 km/s	15.0 km/s	rapid	5.0

Table 4: Initial conditions of the MOBSE simulations. *Column 1*: name of the simulation. *Columns 2 and 3*: 1-D rms of the Maxwellian distribution for ECSN kicks and for CCSN kicks. *Column 4*: SN model. *Column 5*: values of α adopted in the CE formalism.

8 Results

The main goal of this work is to evaluate the influence of metallicity and natal kick on the delay time t_{delay} distribution of compact remnant binaries. The delay time is the time interval between the start of the ZAMS phase of the binary members and the merger event. We calculate the distribution of delay times for merging systems, being N_{merger} the number of merger events at a given t_{delay} bin. The purpose of this analysis is to draw out some results for the merger rate

$$R_{merger} = \frac{number\ of\ mergers}{time}\ . \tag{15}$$

Using a python script, we plotted several histograms with the data resulting from the two simulations. The histograms feature a linear scale in the x axis (t_{delay}) and a logarithmic scale on the y axis ($\log_{10}$ of number of mergers N_{bhb}, N_{bhns} and N_{dns}). All histograms, which are normalized to show the relative frequency on the y axis, feature 50 bins of equal width. Two subset of histograms are plotted, each one with a different fixed parameter: metallicity or natal kick.

8.1 Histograms with fixed metallicity

From the twelve metallicites, we choose to display only six of them (0.0002, 0.0008, 0.002, 0.004, 0.008 and 0.002) to give an overall idea of the impact of the natal kick on t_{delay} distribution. Analyzing all panels of Figure 11, we can give some results.

At low metallicities we do not find a significant impact of the natal kicks on the t_{delay} distribution; while at high metallicities a more considerable dependence on the natal kick may exist, however the total N_{merger} is too low to draw out definitive conclusions. To find more meaningful results in future, we could run additional simulations with more binaries involved.

8.2 Histograms with fixed natal kick

As in the previous Section, we cut some of the metallicities (in this instance 0.012, 0.016 and 0.02 for all panels and in addition 0.008 for the both the BHB and the large kick BHNS panels) to improve the overall readability of the histograms. We focus on the observation of the impact of metallicity

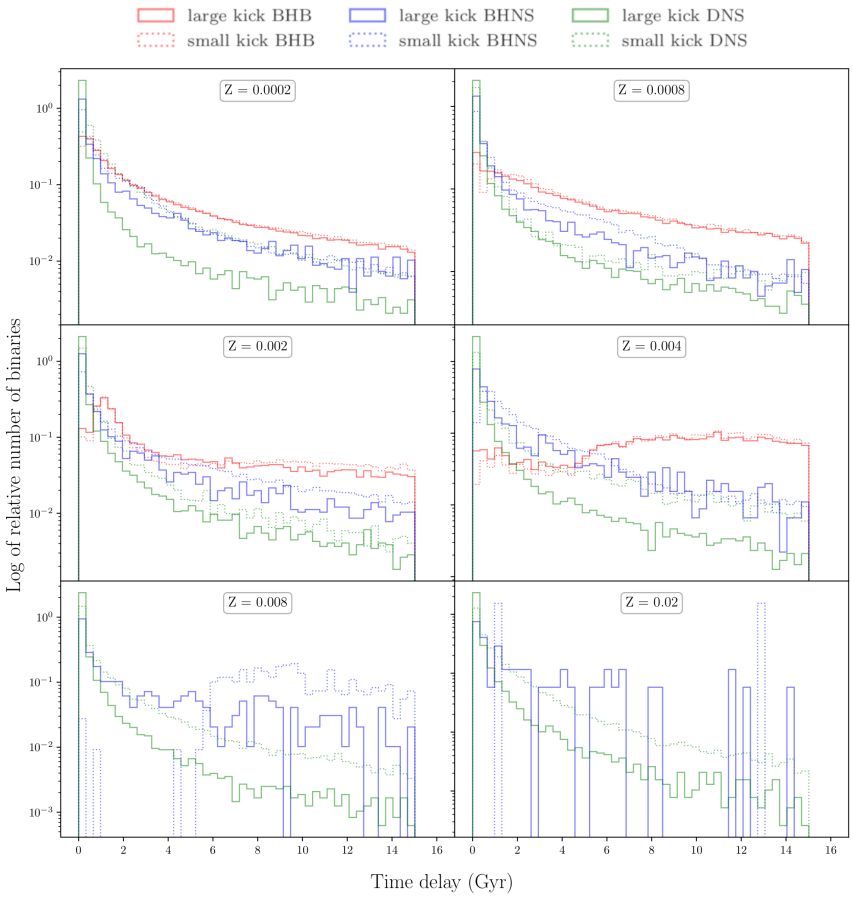

Figure 11: Normalized histograms showing the log of the relative number of mergers for a certain t_{delay}. Each panel features histograms resulting from same metallicity binaries. The small natal kick histograms, resulting from the CC15α5 simulation, are in dashed lines. The bottom two panels do not feature BHB histograms.

on t_{delay} distribution. The analysis of all panels of Figure 12 leads to the following results.

The effects of metallicity on t_{delay} are considerably significant for BHBs systems, while are less relevant on BHNSs and DNS binaries. BHBs seem to have shorter t_{delay} at low metallicity compared to high metallicity. This result has noteworthy implications on the BHB merger rate.

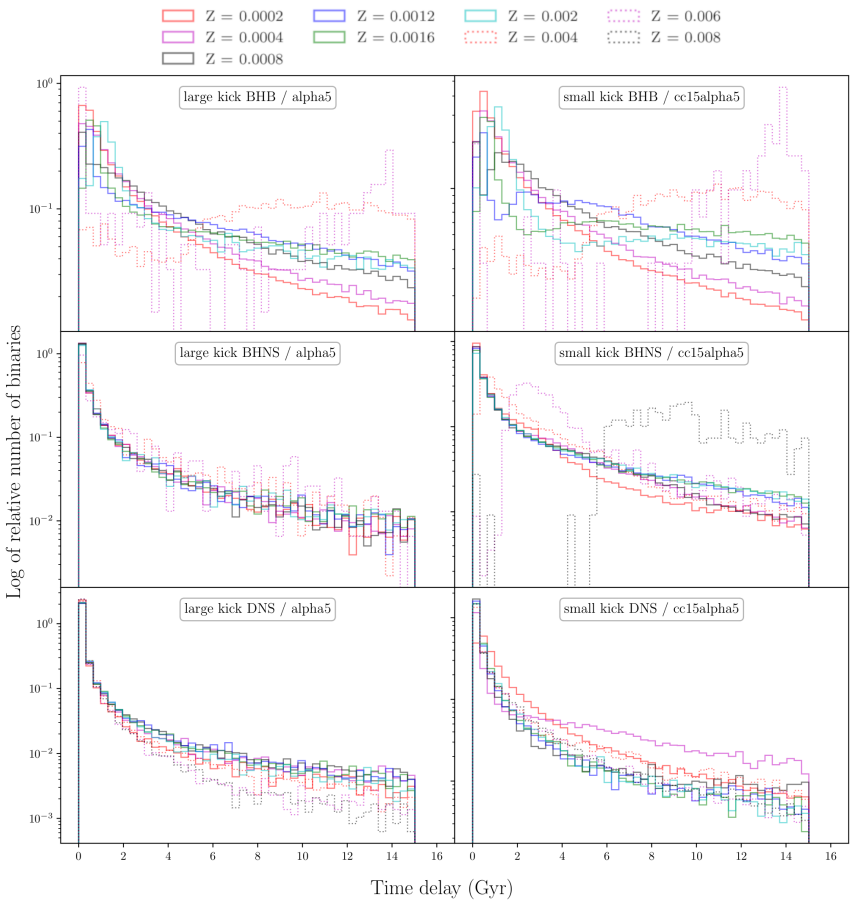

Figure 12: Normalized histograms showing the log of the relative number of mergers for a certain t_{delay}. In the first three panels (top-bottom, left-right), are plotted eight histograms, one for each value of Z. Instead, in the last three panels are plotted nine histograms, one for each value of Z.

9 Conclusions

In the first part of this work, we gave an overview of the *isolated binary scenario*. In the second part, in the light of this model, we analyzed the data resulting from two simulations ran with the *binary synthesis population* code MOBSE. From our analysis we can draw the following conclusions: the delay time does not depend on natal kicks dramatically, while it crucially depends on progenitor's metallicity for BHBs: at low metallicity BHBs seem to have shorter delay times.

Unfortunately, the physical explanation of these conclusions is still uncertain and is subjected to the limitations of our model. Future developments may come from either running simulations involving more binaries or either improving and refining our model, which can be done in many directions. In our scenario several questions remain open. How the gravitational energy released during the core collapse can be converted into kinetic energy of the envelope during a SN explosion? Can we improve the way the SN shock is implemented in the code? How precise is the criterion for the success of a SN based on M_{CO} and M_{fin}? Which is the real scale of the BH natal kicks? Known that the $\alpha\lambda$ approach is too simplified in describing the CE phase, can we create a model more precise that is also implementable?

Future improvements of our understanding of compact object binaries will spring from the answers of these questions, with the objective of refining the astrophysical interpretation of LIGO-Virgo data.

Refernces

[1] Abbott, B. P. et al. (2016). "Observation of Gravitational Waves from a Binary Black Hole Merger". In: *Physical Review Letters* 116.6.

[2] Abbott, B. P. et al. (2019). "GWTC-1: A Gravitational-Wave Transient Catalog of Compact Binary Mergers Observed by LIGO and Virgo during the First and Second Observing Runs". In: *Physical Review X* 9.3.

[3] Abbott, B. P. et al. (2017). "GW170817: Observation of Gravitational Waves from a Binary Neutron Star Inspiral". In: *Physical Review Letters* 119.16.

[4] Lattimer, J. M. (2019). *The Properties of a Black Hole-Neutron Star Merger Candidate*.

[5] Mapelli, M. et al. (2017). "The cosmic merger rate of stellar black hole binaries from the Illustris simulation". In: *Monthly Notices of the Royal Astronomical Society* 472.2, pp. 2422–2435.

[6] Mapelli, M. et al. (2018). "The Host Galaxies of Double Compact Objects Merging in the Local Universe". In: *Monthly Notices of the Royal Astronomical Society* 481.4, pp. 5324–5330.

[7] Vink, J. S., de Koter, A., and Lamers, H. J. G. L. M. (2001). "Mass-loss predictions for O and B stars as a function of metallicity". In: *Astronomy and Astrophysics* 369, pp. 574–588.

[8] Belczynski, K. et al. (2010). "On the Maximum Mass of Stellar Black Holes". In: *The Astrophysical Journal* 714, pp. 1217–1226.

[9] Vink, J. S., Jorick, S., and de Koter, A. (2005). "On the metallicity dependence of Wolf-Rayet winds". In: *Astronomy and Astrophysics* 442.2, pp. 587–596.

[10] Chen, Y. et al. (2015). "Parsec evolutionary tracks of massive stars up to 350 $M_{\odot}$ at metallicities $0.0001 \leq Z \leq 0.04$". In: *Monthly Notices of the Royal Astronomical Society* 452.1, pp. 1068–1080.

[11] Limongi, M. (2017). "Supernovae from Massive Stars". In: *Handbook of Supernovae*, pp. 513–565.

[12] Mapelli, M. (2018). *Astrophysics of stellar black holes*.

[13] Janka, H.-T. (2012). "Explosion Mechanisms of Core-Collapse Supernovae". In: *Annual Review of Nuclear and Particle Science* 62.1, pp. 407–451.

[14] Chandrasekhar, S. (1931). "The Maximum Mass of Ideal White Dwarfs". In: *The Astrophysical Journal* 74, p. 81.

[15] Fowler, W. A. and Hoyle, F. (1964). "Neutrino Processes and Pair Formation in Massive Stars and Supernovae". In: *The Astrophysical Journal, Supplement* 9, p. 201.

[16] Barkat, Z., Rakavy, G., and Sack, N. (1967). "Dynamics of Supernova Explosion Resulting from Pair Formation". In: *Physical Review Letters* 18.10, pp. 379–381.

[17] Rakavy, G. and Shaviv, G. (1967). "Instabilities in Highly Evolved Stellar Models". In: *The Astrophysical Journal* 148, p. 803.

[18] Woosley, S. E. (2017). "Pulsational Pair-instability Supernovae". In: *The Astrophysical Journal* 836.2, p. 244.

[19] Bethe, H. A. and Wilson, J. R. (1985). "Revival of a stalled supernova shock by neutrino heating". In: *Astrophysical Journal* 295, pp. 14–23.

[20] Fryer, C. L. et al. (2012). "Compact Remnant Mass Function: Dependence on the Explosion Mechanism and Metallicity". In: *The Astrophysical Journal* 749.1, p. 91.

[21] Müller, B. (2016). "The Core-Collapse Supernova Explosion Mechanism". In: *Proceedings of the International Astronomical Union* 12.S329, pp. 17–24.

[22] O'Connor, E. and Ott, C. D. (2011). "Blach Hole Formation in Failing Core-Collapse Supernovae". In: *The Astrophysical Journal* 730.2, p. 70.

[23] Heger, A. et al. (2003). "Massive Star Evolution Through the Ages". In: *From Twilight to Highlight: The Physics of Supernovae*, pp. 3–12.

[24] Spera, M., Mapelli, M., and Bressan, A. (2015). "The Mass Spectrum of Compact Remnants from the PARSEC Stellar Evolution Tracks". In:

[25] Spera, M. and Mapelli, M. (2017). "Very massive stars, pair-instability supernovae and intermediate-mass black holes with the sevn code". In: *Monthly Notices of the Royal Astronomical Society* 470.4, pp. 4739–4749.

[26] Giacobbo, N. and Mapelli, M. (2018a). "The Impact of Electron-Capture Supernovae on Merging Double Neutron Stars". In: *Monthly Notices of the Royal Astronomical Society* 482.2, pp. 2234–2243.

[27] Hobbs, G. et al. (2005). "A statistical study of 233 pulsar proper motions". In: *Monthly Notices of the Royal Astronomical Society* 360.3, pp. 974–992.

[28] Mirabel, F. (2017). "The Formation of Stellar Black Holes". In: *New Astronomy Reviews* 78, pp. 1–15.

[29] Hurley, J. R., Tout, C. A., and Pols, O. R. (2002). "Evolution of Binary Stars and the Effect of Tides on Binary Populations". In: *Monthly Notices of the Royal Astronomical Society* 329.4, pp. 897–928.

[30] Eggleton, P. P. (1983). "Approximations to the Radii of Roche lobes". In: *The Astrophysical Journal* 268, pp. 368–369.

[31] Portegies Zwart, S. F. and Verbunt, F. (1996). "Population Synthesis of High-Mass Binaries". In: *Astronomy and Astrophysics* 309, pp. 179–196.

[32] Tout, C. A. et al. (1997). "Rapid Binary Star Evolution for N-body Simulations and Population Synthesis". In: *MNRAS* 291.4, pp. 732–748.

[33] Webbink, R. F. (1984). "Double White Dwarfs as Progenitors of R Coronae Borealis Stars and Type I Supernovae." In: *The Astrophysical Journal* 277, pp. 355–360.

[34] Ivanova, N. et al. (2013). "Common Envelope Evolution: where we stand and how we can move forward". In: *The Astronomy and Astrophysics Review* 21.1.

[35] Xu, X.-J. and Li, X.-D. (2010). "On the Binding Energy Parameter λ of Common Envelope Evolution". In: *The Astrophysical Journal* 716.1, pp. 114–121.

[36] Giacobbo, N., Spera, M., and Mapelli, M. (2018). "Merging black hole binaries: the effects of progenitor's metallicity, mass-loss rate and Eddington factor". In: *Monthly Notices of the Royal Astronomical Society* 474.3, pp. 2959–2974.

[37] Giacobbo, N. and Mapelli, M. (2018b). "The progenitors of compact-object binaries: impact of metallicity, common envelope and natal kicks". In: *MNRAS* 480, pp. 2011–2030.

[38] Kroupa, P. (2001). "On the variation of the initial mass function". In: *Monthly Notices of the Royal Astronomical Society* 322.2, pp. 231–246.

[39] Sana, H. et al. (2012). "Binary Interaction Dominates the Evolution of Massive Stars". In: *Science* 337, p. 444.